

Journal Pre-proofs

Comparative study of WSe₂ thin films synthesized via pre-deposited WO₃ and W precursor material selenization

Kevon Kadiwala, Edgars Butanovs, Andrejs Ogurcovs, Martins Zubkins, Boris Polyakov

PII: S0022-0248(22)00252-4

DOI: <https://doi.org/10.1016/j.jcrysgr.2022.126764>

Reference: CRY 126764

To appear in: *Journal of Crystal Growth*

Received Date: 8 January 2022

Revised Date: 22 May 2022

Accepted Date: 8 June 2022

Please cite this article as: K. Kadiwala, E. Butanovs, A. Ogurcovs, M. Zubkins, B. Polyakov, Comparative study of WSe₂ thin films synthesized via pre-deposited WO₃ and W precursor material selenization, *Journal of Crystal Growth* (2022), doi: <https://doi.org/10.1016/j.jcrysgr.2022.126764>

This is a PDF file of an article that has undergone enhancements after acceptance, such as the addition of a cover page and metadata, and formatting for readability, but it is not yet the definitive version of record. This version will undergo additional copyediting, typesetting and review before it is published in its final form, but we are providing this version to give early visibility of the article. Please note that, during the production process, errors may be discovered which could affect the content, and all legal disclaimers that apply to the journal pertain.

© 2022 Published by Elsevier B.V.



Comparative study of WSe₂ thin films synthesized via pre-deposited WO₃ and W precursor material selenization

*Kevon Kadiwala**, *Edgars Butanovs*, *Andrejs Ogurcovs*, *Martins Zubkins*, *Boris Polyakov*

Institute of Solid State Physics, University of Latvia, Kengaraga street 8, Riga, Latvia, LV-1063

*e-mail: kevon.kadiwala@cfi.lu.lv

Abstract

Layered two-dimensional (2D) materials, such as p-type WSe₂, are potential key materials in the manufacture of the next generation electronic devices. One of the remaining main challenges is the large area growth of high-quality films. A potential large-scale 2D WSe₂ synthesis method is conversion (selenization) of a pre-deposited sacrificial precursor coating. However, its use is still limited, mainly due to a lack of understanding the growth mechanisms involved. Here, we have studied and compared properties of thin crystalline WSe₂ films prepared via selenization of sputter-deposited sacrificial WO₃ and W films. Surface morphology of the as-grown films was studied using a scanning electron microscope complemented with an atomic force microscope. The structure and chemical composition were confirmed by X-ray diffraction and micro-Raman spectroscopy, respectively. On-chip photoconductive devices were made using the standard photolithography process, and their photoresponse was investigated with 405 nm wavelength light. For the electrical characterization, field effect transistors (FETs) were made to measure output and transfer curves. The results obtained give insight into the growth of crystalline WSe₂ via sacrificial film selenization.

Keywords

B1. tungsten diselenide; B1. transitional metal dichalcogenides; A3. thin films; A3. chemical vapor transport; B3. Photolithography

1. Introduction

Transition metal dichalcogenides (TMDs) have gained quite a lot of attention in recent years, mainly due to their nature of being layered van der Waals (vdW) materials [1]. In bulk, they do not exhibit any exclusive characteristics for electronics applications, but when reduced to two-dimensional (2D) form, they have displayed unparalleled properties which are suitable for replacing the conventional semiconducting materials [2–6]. Exploring the potential applications of these semiconducting materials is currently an active topic of research which generally includes demonstration of their use in the fields of photovoltaic cells, field-effect transistors, phototransistors, production of H₂ via water splitting, Schottky diodes, and more [7–14]. The reason why these materials have sparked such research interest is the availability of intrinsic p-type and n-type of 2D materials. Most of the reported TMDs are n-type semiconductors (e.g. MoS₂) by nature, however, WSe₂ is currently being studied extensively for its p-type characteristics [1,2,4,15–19]. Employing this property of WSe₂ and combining it with other n-type TMDs, using the weak vdW force, opens up possibilities for fabrication of the next generation of heterostructures [8–11,20–22].

WSe₂ has a crystal structure comprised of Se-W-Se layers weakly bonded via vdW force, generating a sandwich-like form. These three atomic layers are packed in hexagon shape, and in turn they make a monolayer of WSe₂ [23]. These layers of WSe₂ are highly prone to randomly distributed defects such as Se atom vacancy and W atom vacancy [5,24,25], which in turn affects the quality and the properties of the crystals. The electronic energy band structure of this material changes with the number of layers stacked on each other [26]. WSe₂ shows indirect bandgap when in the bulk state, but that changes to direct bandgap when number of layers is decreased to one [1]. To achieve this high quality of monolayer WSe₂, various methods have been proposed and demonstrated including

different types of chemical vapour deposition (CVD) methods [14], pulsed-laser deposition (PLD) [27] and atomic layer deposition (ALD) [28].

In this work, we report the synthesis of WSe₂ by the method of chemical vapour transport (CVT) in which we have used two different sources of pre-deposited sacrificial precursor films – WO₃ and W metal. The reason for this study was to compare the synthesized WSe₂ crystalline films from each precursor material and understand how they affect the different properties of the film. The CVT method is one of the most efficient, widely used, and up-scalable 2D material synthesis techniques available. Therefore, WSe₂ films were also synthesized using that method, keeping in mind possible upscaling in the future. To showcase the photoelectric properties of the synthesized films, on-chip devices are also demonstrated.

2. Experimental details

2.1. Tungsten diselenide film synthesis:

Sacrificial precursor films with varying thicknesses, from 3 nm to 50 nm, were deposited on oxidized silicon wafers SiO₂/Si (100) (Semiconductor Wafer, Inc.) by reactive DC magnetron sputtering of a metallic tungsten target in a mixed Ar/O₂ atmosphere ($5 \cdot 10^{-3}$ torr, 30 sccm Ar, and 20 sccm O₂ gas flow at 300 W DC power). After the precursor material deposition, synthesis of WSe₂ was performed from W metal film and WO₃ film using CVT. The CVT setup consists of a horizontal open-end quartz tube reactor. For the procedure, selenium powder was loaded in a ceramic boat at one end of the quartz tube. The vapour of selenium was transported downstream to the W/WO₃ precursor material on a silicon substrate using the carrier gas mixture: 5% Ar/H₂ in the

case of WO_3 and 35% Ar/H_2 in the case of W. The temperatures (ranging from 600 to 850 °C) were held constant for 20 min, followed by uninterrupted cooling to the room temperature.

The synthesized films were studied under a scanning electron microscope (SEM-FIB Lyra, Tescan) and a Park NX10 (Park Systems) atomic force microscope (AFM) for the surface morphology. The phase compositions of the samples were studied using X-ray diffraction (XRD, powder diffractometer Rigaku Miniflex 600) with monochromatic $\text{Cu K}\alpha$ irradiation ($\lambda = 1.5406 \text{ \AA}$), and the spectra were analysed using PDXL2 software. Micro-Raman spectroscopy measurements were performed using a TriVista 777 confocal Raman system (Princeton Instruments) equipped with an upright Olympus microscope with an Olympus UISe MPlanN 100x/0.90 objective, a continuous-wave single-frequency diode-pumped laser Cobolt Samba 150 ($\lambda = 532 \text{ nm}$), and an Andor iDus DV420A-OE CCD camera. For the electrical characterization, silicon substrates (100) with a 300 nm oxide layer (Semiconductor Wafer, Inc.) were used with a separate design configuration, and the measurements were carried out using two (Keithley 2400) source-meter units. Transfer characteristics ($I_{\text{DS}}-V_{\text{GS}}$) were measured at gate voltages ranging from +30V to -30V and source-drain voltages of 0V to 5V, with a total acquisition time of 24 seconds for each curve. Output characteristics ($I_{\text{DS}}-V_{\text{DS}}$) were measured similarly with gate bias voltages ranging from 0V to -20V and source-drain voltages ranging from 0V to 5V, with a total acquisition time of 24 seconds for each output curve.

2.2 On-chip photosensor device fabrication:

Fabrication of on-chip devices had a few extra steps involved compared to the synthesis of plain WSe_2 films on silicon samples. The steps are graphically illustrated in *Fig. 1*. Using the conventional photolithography (spin-coating, exposure, development), the first layer of mask was created for depositing the precursor material in specific regions with magnetron sputtering. After deposition of

the desired precursor material, the mask was removed applying the standard lithography lift-off procedure. Conversion from precursor material W/WO₃ to WSe₂ took place afterwards using the CVT method, and then another mask was deposited on top of the WSe₂ films using the previously used standard lithography process for the deposition of the electric contacts to fabricate the on-chip devices. These fabricated devices were used for the photoelectric measurements.

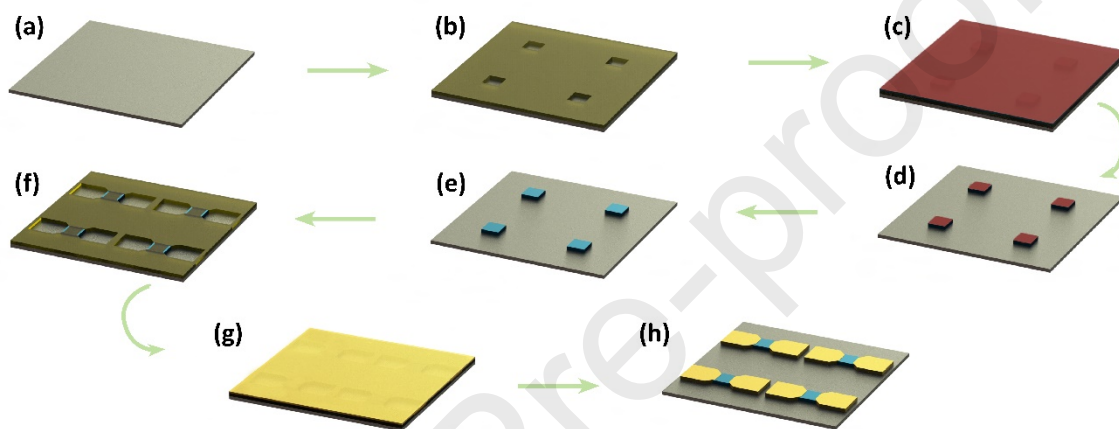


Fig. 1. Schematic of the process of on-chip device fabrication. First the SiO₂/Si substrate is cleaned using acetone and isopropanol (a), then the first mask is made using the standard photolithography process (b) on which precursor material is deposited (c). After first mask lift-off, the precursor material film is in the desired pattern (d) which is subsequently selenized (e). Afterwards, the second photoresist mask is deposited (f) for the deposition of contact material (Cr ~ 5 nm, Ag ~ 95 nm, Al ~ 50 nm) using the thermal evaporation method (g) followed by lift-off to obtain the photoconductor device array on a chip (h).

2.3 Device measurements:

Photoresponse and the current-voltage (I-V) curves were measured for the fabricated devices using a two-contact microprobe station connected to a low-noise current preamplifier (SR570, Stanford

Research Systems) and an oscilloscope (TDS2004B, Tektronix). A 405 nm wavelength semiconductor diode laser (CNI Laser) with 1 W/cm^2 was the illumination source for the photo-response measurements. An optical beam shutter (Thorlabs SH05) was used for time-resolved measurements. All the measurements were performed at room temperature and in air.

3. Results and discussion

Various thicknesses of the deposited precursor materials (WO_3 and W) ranging from 3 nm to 40 nm

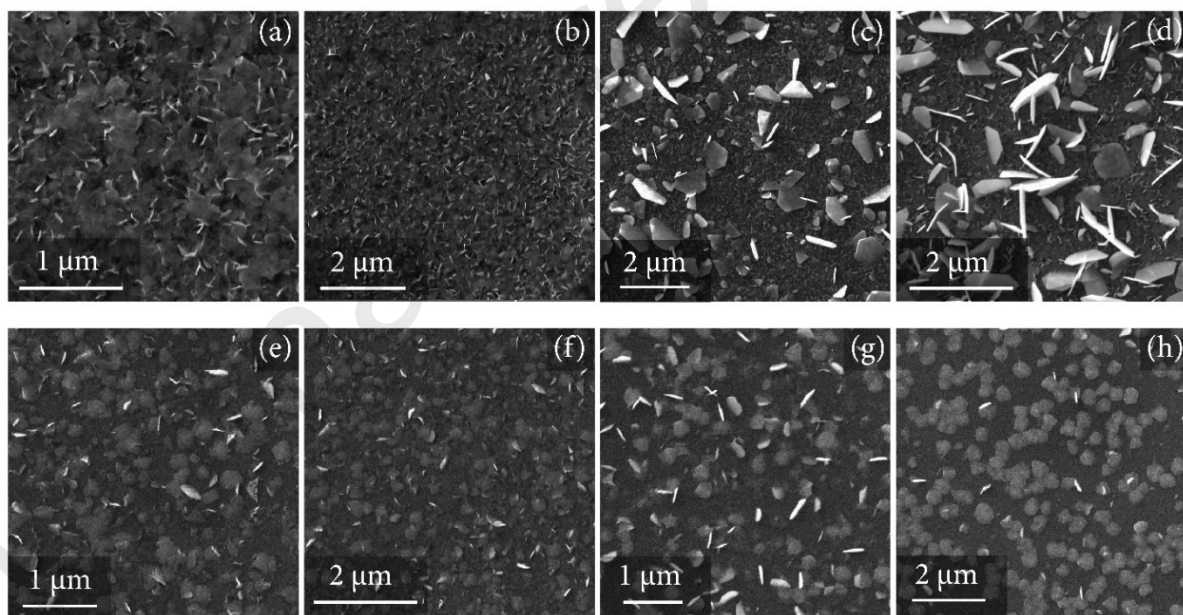


Fig. 2. Scanning electron microscope images at different magnifications of WSe_2 films made from a WO_3 precursor at 700 °C (a,b) and 800 °C (c,d) and from a W metal precursor at 700 °C (e,f) and 800 °C (g,h).

were tested. The attempt to make a 3 nm film resulted in forming an island structure instead of a

Journal Pre-proofs

continuous film. Optimally, the continuous and homogeneous yet thinnest films were about 10 nm

in thickness and above. SEM was used to study the as-grown WSe₂ film's morphology. Films

synthesized from the WO_3 precursor material typically had larger crystals, reaching up to a diameter

Journal Pre-proofs

of 1 μm at a high temperature (800 $^{\circ}\text{C}$), while at a lower temperature (700 $^{\circ}\text{C}$), the crystals did not

Journal Pre-proofs

seem to have distinctive boundaries (*see Fig. 2(a-d)*). Above 800 °C the films started to sublime,

while below 700 °C the films showed no formation of WSe₂ crystals. However, for the films made

from a W metal precursor, the crystals demonstrated distinctive boundaries, but they were

Journal Pre-proofs

comparatively smaller in size – growing up to the diameter of 0.5 μm regardless of the CVT process

Journal Pre-proofs

temperature (see Fig. 2(e-h)). WSe₂ films also had a distinctive difference in the average crystals

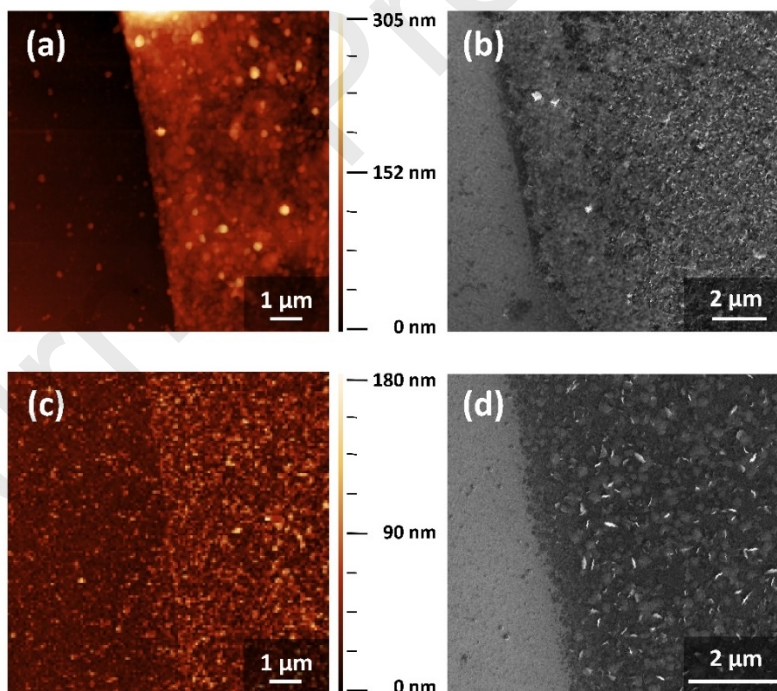


Fig. 3. Atomic force microscope (AFM) Z-drive images of WSe₂ films made from a WO₃ precursor (a) and from a W metal precursor (c) showing the difference between film surfaces and further complimented by SEM images of the same samples in the respective order of (b) and (d).

size. On average, crystals grown from the W metal precursor were of similar diameter (0.3 – 0.5

Journal Pre-proofs

μm), whereas the crystals grown from the WO_3 precursor had a significant variance in diameter (0.2

Journal Pre-proofs

– 1.5 μm). The reason for the larger out-of-plane WSe_2 crystal growth at 700-800 $^\circ\text{C}$ compared to

Journal Pre-proofs

the W metal species is presumably due to the higher volatility and diffusivity of the WO_3 species. Furthermore, the surface morphology of the films depends on the precursor material, which is visible in AFM images and complemented by SEM images (*see Fig. 3*). WSe_2 films synthesized from the WO_3 precursor material showcased more crystals growing out-of-plane compared to the films synthesized from W metal precursor. Z-drive images (*Fig. 3(a,c)*) obtained from AFM, show a few crystals coming out in random distribution, whereas the film grown from W metal has better distribution of crystals with a comparatively flatter surface. This out-of-plane crystal growth could be caused by evaporation of the WO_3 precursor film followed by selenization in the vapour phase

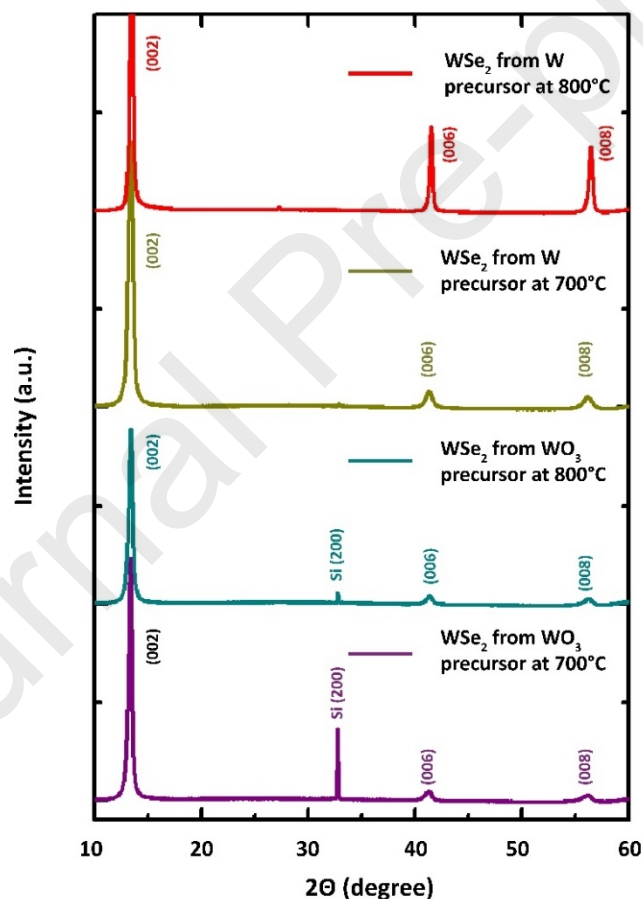


Fig. 4. X-ray diffraction patterns of WSe_2 films from both precursors (WO_3 and W) at different temperatures, 700 °C and 800 °C, show peaks confirming the phase of the synthesized WSe_2 film. and as-formed WSe_2 re-deposition, leading to growth of crystals.

The presence of different phases in WSe_2 films on $\text{Si}(100)/\text{SiO}_2$ were checked using XRD measurements. *Fig. 4* shows the XRD patterns for films synthesized from WO_3 and W metal at different temperatures of 700 °C and 800 °C. All patterns indicate crystalline films of WSe_2 (ICDD-

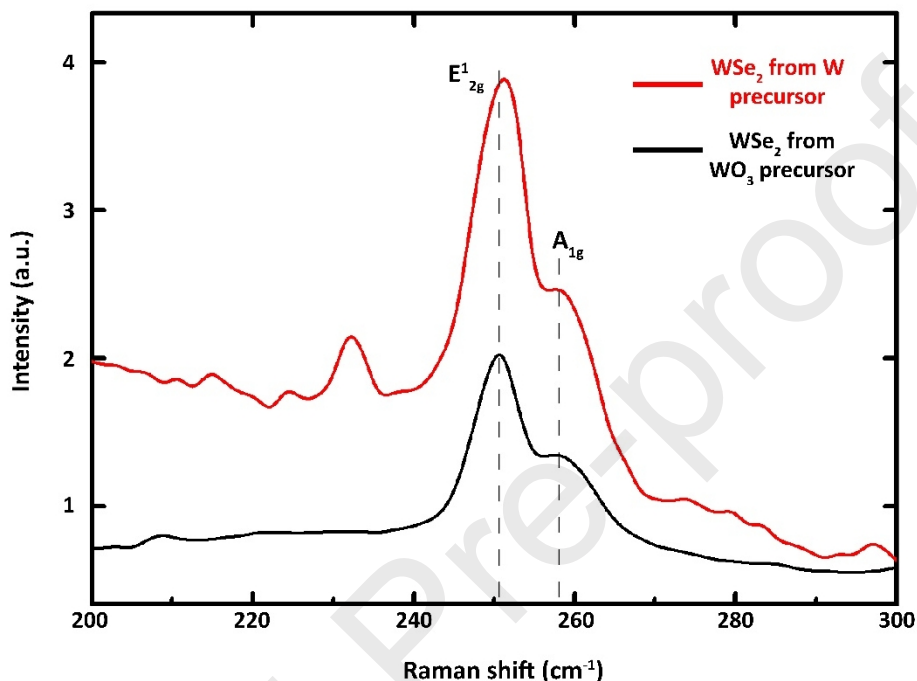


Fig. 5. Raman spectra of WSe_2 thin films synthesized from both precursors (WO_3 and W) using CVT method showing the peaks respective to E_{2g}^1 and A_{1g} vibrational modes.

PDF #38-1388). No other phases were detected during the measurement. In *Fig. 4*, the peak at 33° is ascribed to the diffraction in the $\text{Si}(100)$ substrate (forbidden $\text{Si}(200)$ reflection). To compliment these results, room temperature micro-Raman measurements were also performed on the synthesized films. The Raman peaks (*Fig. 5*) observed around 250.2 and 259 cm^{-1} are attributed to the in-plane (E_{2g}^1) and out-of-plane (A_{1g}) vibrational modes of WSe_2 , therefore confirming the formation of WSe_2 [26]. XRD patterns and Raman measurements of as-grown films confirm the conversion of precursor materials to WSe_2 crystals using the CVT process, which makes it a viable method to obtain WSe_2 thin films.

As shown in *Fig. 6(a,b)*, in the first, step various sized continuous WSe₂ films were prepared using

photolithography to make devices with varying gap widths between the two electrodes, ranging

Journal Pre-proofs

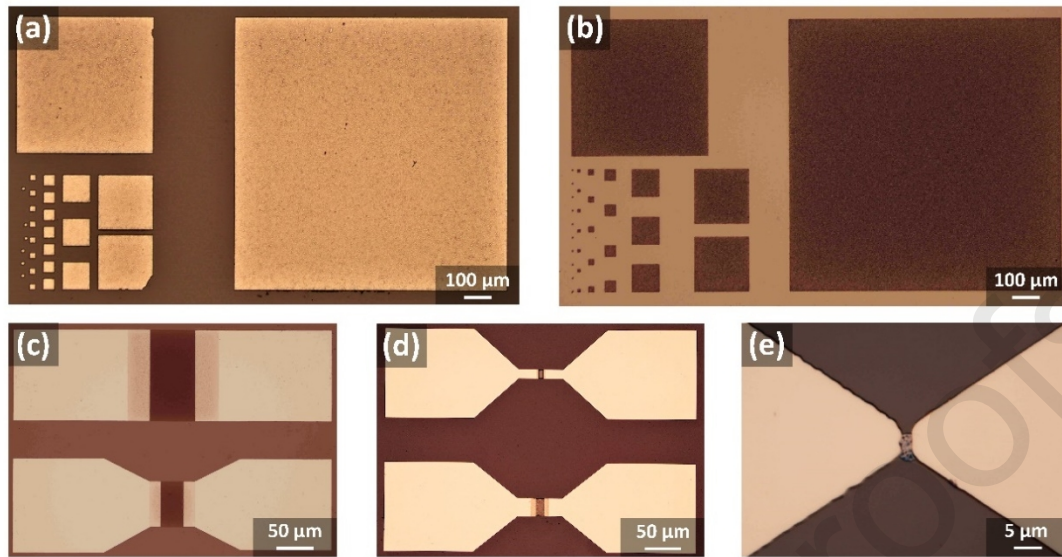


Fig. 6. Optical images of the synthesized patterned WSe₂ films made by photolithography (a,b), and devices with various gap widths between the two electrodes were fabricated (c-e) using WSe₂ films. from 250 μm to 2 μm (Fig. 6(c-e)). Fig. 7(a-c) shows the photoelectric characteristics of the WSe₂

films synthesized from WO_3 , and *Fig. 7(d-f)* shows the photoelectric characteristics of the films

synthesized from W metal precursor. Dark state current–voltage (I–V) for both the films can be seen

Journal Pre-proofs

to exhibit linear behaviour, suggesting that Ohmic contacts may have been formed. The devices

Journal Pre-proofs

were illuminated with a 405 nm wavelength light source in a periodic fashion to study their photo-

Journal Pre-proofs

response properties, as shown in *Fig. 7(e,h)*. The devices were also tested with 532 nm and 660 nm

light. However, no sensitivity from the devices was observed. On-off measurements demonstrate a rapid and repeatable increase and decrease of current (rise and fall times), below 20 ms, when the

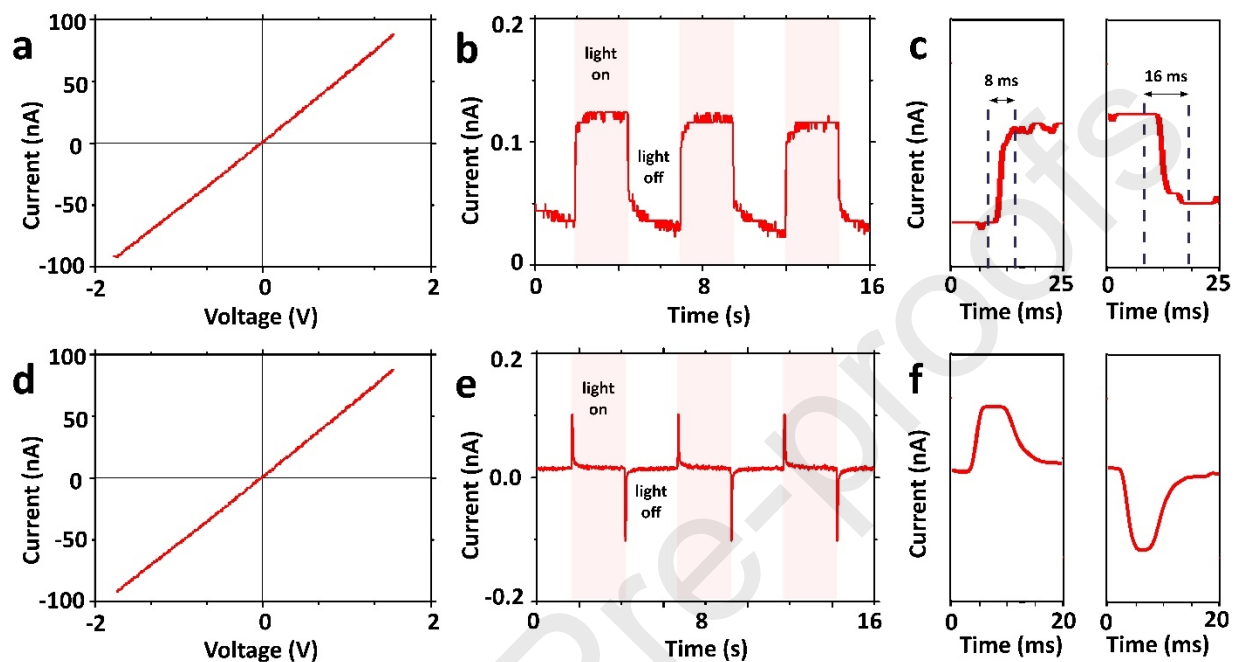


Fig. 7. WSe₂ two-terminal photoconductor devices prepared from WO₃ and W metal as the precursor materials, respectively, showing dark state I–V characteristics (a,d), on-off response (b,e), and response time (c,f) measurements at 2 V bias voltage and 1 W/cm² light intensity with a 405 nm wavelength light source.

light source is turned on and off, respectively. This demonstrates good reversibility of the devices. Furthermore, it was observed that WSe₂ film made from the W metal precursor did not exhibit stable persistent photocurrent. When exposed to light, transient current can be observed, quickly followed by return to dark current level. Similarly, when the light source is turned off, it shows similar behaviour with a negative transient current at the start. This transient current can occasionally be observed for nanoscale photodetector devices, and it is attributed to charge trapping/de-trapping in semiconductor/electrode interfaces and to space-charge effects [29,30].

WSe₂ 2D crystals are highly prone to various defects [5,24], such as selenium vacancies, which have been shown to degrade photoelectric properties of WSe₂ [31]. These defects might cause the poor photoelectric performance for devices made from a W precursor. On the other hand, the films made

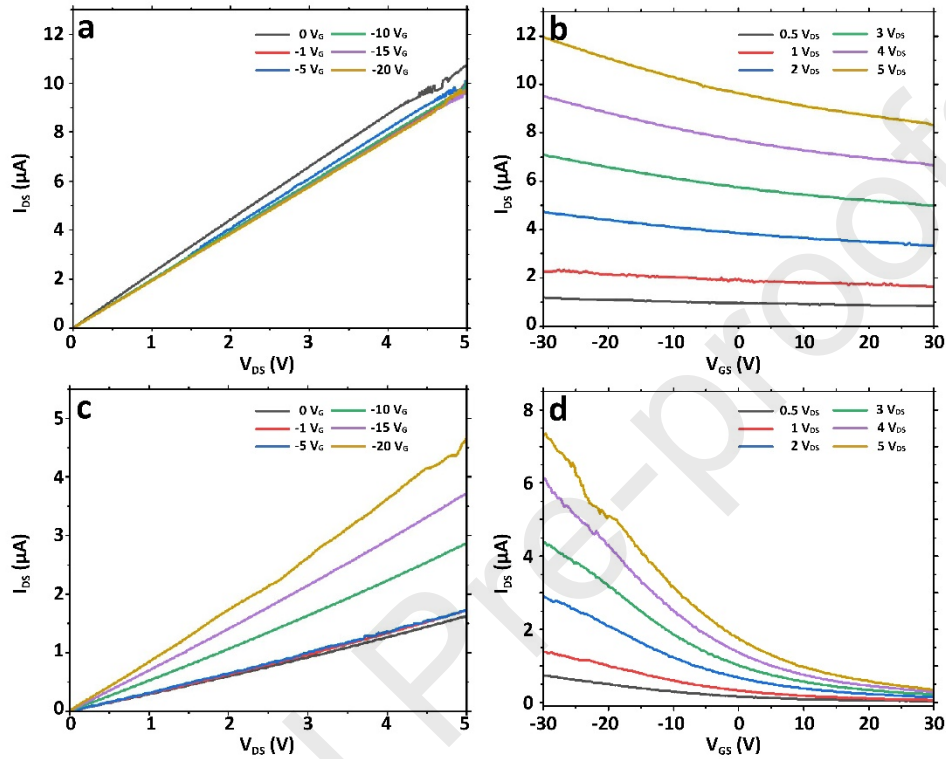


Fig. 8. WSe₂ two-terminal photoconductor devices, prepared from WO₃ and W metal as the precursor (I_{DS} - drain source current, V_{DS} -drain source bias voltage, V_{GS} - gate source bias voltage)

from a WO₃ precursor material exhibit better photoelectric properties because WO₃ might be providing oxygen impurities during the formation of the crystals. Selenium vacancy passivation with oxygen atoms has been previously demonstrated to restore/enhance photodetector performance [31]. In contrast, films made from W metal lack such oxygen atoms to passivate the selenium vacancies, leaving the films with degraded photoelectric properties.

For the electrical characterization of these films, field effect transistors (FETs) were made to measure the output and transfer curves (see Fig. 8). The output curve (*Fig 8(a)*) for W metal films

converted to WSe_2 has a minor reaction to the gate bias potential, which suggests incomplete conversion of W film to WSe_2 . The remaining metal phase is acting as a shunt resistance for the semiconducting layers of WSe_2 . Transfer curves (*Fig 8(b)*) at higher V_{DS} and negative V_{GS} can be noticed to have conductivity enhancement caused by the field-effect of WSe_2 layers, thus indicating that a majority of the charge carriers in these layers are holes. *Fig. 8(c,d)* represents the output and transfer characteristics of the WSe_2 sample converted from the WO_3 precursor material. These devices exhibit a much stronger field-effect compared to the previous sample, and negative 'ON' voltage indicates p-type conductivity. Nonlinear behaviour of the output curves between -5 V and -10 V gate voltage (*Fig 8(c)*) can be caused by a small Schottky barrier at the metal/semiconductor junction due to the difference between the work function of Cr and WSe_2 . Lowering V_{GS} from +30 V to -30 V results in an increase of I_{DS} by 95.9% at 5 V source-drain voltage (*Fig 8(d)*) compared to 31.6% for the *Fig 8(b)*. This indicates that the synthesis via CVT of WSe_2 from precursor WO_3 is better compared to W for the electrical properties as well.

4. Conclusions

In this work, we demonstrated, for the first time, a comparison of WSe_2 thin films made from two different pre-deposited precursor materials, WO_3 and W metal, using the CVT method at atmospheric pressure. As found during the characterization, SEM and AFM images showed the films grown from the W metal precursor had significantly lower surface roughness than the films grown from the WO_3 precursor. For the films made from the W precursor, crystal sizes were noticeably smaller ($\sim 0.4 \mu\text{m}$) in comparison to the films made from WO_3 ($\sim 0.8 \mu\text{m}$) which had crystal growth in a random orientation. Photoelectric measurements revealed that, despite having the out-of-plane crystal growth on the film from the WO_3 precursor, WO_3 films showed higher

photocurrent and stability, which was not the case with planar crystals grown from the W metal precursor. From the point of view of electrical properties, both films exhibited p-type conductivity. However, the films made from the WO_3 precursor showed better performance compared to the films made from the W metal precursor; indicating that WO_3 is a better precursor material than W metal when using the CVT approach for the synthesis of WSe_2 .

Declaration of competing interest

There are no conflicts of interest to declare.

Credit authorship contribution statement

Kevon Kadiwala: Methodology, Validation, Investigation, Visualization, Writing - original draft. Edgars Butanovs: Methodology, Investigation, Writing – review & editing. Martins Zubkins: Investigation. Andrejs Ogurcovs: Investigation. Boris Polyakov: Conceptualization, Supervision, Investigation, Writing - review & editing.

Acknowledgements

Financial support provided by Scientific Research Project for Students and Young Researchers Nr. SJZ/2020/04 realized at the Institute of Solid State Physics, University of Latvia is greatly acknowledged. Institute of Solid State Physics, University of Latvia as the Centre of Excellence has

received funding from the European Union's Horizon 2020 Framework Programme H2020-WIDESPREAD-01-2016-2017-TeamingPhase2 under grant agreement No. 739508, project CAMART². Authors are grateful to Jevgenijs Gabrusenoks for micro-Raman measurements.

References

- [1] Q. Cheng, J. Pang, D. Sun, J. Wang, S. Zhang, F. Liu, Y. Chen, R. Yang, N. Liang, X. Lu, Y. Ji, J. Wang, C. Zhang, Y. Sang, H. Liu, W. Zhou, WSe₂ 2D p-type semiconductor-based electronic devices for information technology: Design, preparation, and applications, *InfoMat.* 2 (2020) 656–697. <https://doi.org/10.1002/inf2.12093>.
- [2] H.S. Arora, R. Polski, Y. Zhang, A. Thomson, Y. Choi, H. Kim, Z. Lin, I.Z. Wilson, X. Xu, J.H. Chu, K. Watanabe, T. Taniguchi, J. Alicea, S. Nadj-Perge, Superconductivity in metallic twisted bilayer graphene stabilized by WSe₂, *Nature.* 583 (2020) 379–384. <https://doi.org/10.1038/s41586-020-2473-8>.
- [3] Z. Wu, W. Zhao, J. Jiang, T. Zheng, Y. You, J. Lu, Z. Ni, Defect Activated Photoluminescence in WSe₂ Monolayer, *J. Phys. Chem. C.* 121 (2017) 12294–12299. <https://doi.org/10.1021/acs.jpcc.7b03585>.
- [4] W.T. Hsu, L.S. Lu, D. Wang, J.K. Huang, M.Y. Li, T.R. Chang, Y.C. Chou, Z.Y. Juang, H.T. Jeng, L.J. Li, W.H. Chang, Evidence of indirect gap in monolayer WSe₂, *Nat. Commun.* 8 (2017) 1–7. <https://doi.org/10.1038/s41467-017-01012-6>.
- [5] Y.J. Zheng, Y. Chen, Y.L. Huang, P.K. Gogoi, M.Y. Li, L.J. Li, P.E. Trevisanutto, Q. Wang, S.J. Pennycook, A.T.S. Wee, S.Y. Quek, Point Defects and Localized Excitons in 2D WSe₂, *ACS Nano.* 13 (2019) 6050–6059. <https://doi.org/10.1021/acsnano.9b02316>.
- [6] Y. Wang, L. Zhang, S. Lv, F. Zhang, Q. Sui, L. Jia, M. Jiang, In-situ variable reflectance spectra model of two-dimensional material prepared by CVD, *J. Cryst. Growth.* 559 (2021) 126034. <https://doi.org/10.1016/j.jcrysgro.2021.126034>.
- [7] P.M. Pataniya, C.K. Zankat, M. Tannarana, A. Patel, S. Narayan, G.K. Solanki, K.D. Patel, P.K. Jha, V.M. Pathak, Photovoltaic activity of WSe₂/Si hetero junction, *Mater. Res. Bull.* 120 (2019). <https://doi.org/10.1016/j.materresbull.2019.110602>.
- [8] G.H. Shin, C. Park, K.J. Lee, H.J. Jin, S.Y. Choi, Ultrasensitive Phototransistor Based on WSe₂-

MoS₂/van der Waals Heterojunction, *Nano Lett.* 20 (2020) 5741–5748.

<https://doi.org/10.1021/acs.nanolett.0c01460>.

[9] F. Hu, L. Tao, H. Ye, X. Li, X. Chen, ZnO/WSe₂ vdW heterostructure for photocatalytic water splitting, *J. Mater. Chem. C* 7 (2019) 7104–7113. <https://doi.org/10.1039/c9tc00573k>.

[10] J. Sun, Y. Wang, S. Guo, B. Wan, L. Dong, Y. Gu, C. Song, C. Pan, Q. Zhang, L. Gu, F. Pan, J. Zhang, Lateral 2D WSe₂ p–n Homojunction Formed by Efficient Charge-Carrier-Type Modulation for High-Performance Optoelectronics, *Adv. Mater.* 32 (2020) 1–9. <https://doi.org/10.1002/adma.201906499>.

[11] P. Lin, J. Yang, Tunable WSe₂/WS₂ van der Waals heterojunction for self-powered photodetector and photovoltaics, *J. Alloys Compd.* 842 (2020) 155890. <https://doi.org/10.1016/j.jallcom.2020.155890>.

[12] S.J. Yang, K.T. Park, J. Im, S. Hong, Y. Lee, B.W. Min, K. Kim, S. Im, Ultrafast 27 GHz cutoff frequency in vertical WSe₂ Schottky diodes with extremely low contact resistance, *Nat. Commun.* 11 (2020) 1–9. <https://doi.org/10.1038/s41467-020-15419-1>.

[13] Butanovs, E., Kuzmin, A., Butikova, J., Vlassov, S. & Polyakov, Synthesis and characterization of ZnO/ZnS/MoS₂ core-shell nanowires, *J. Cryst. Growth.* (2017) 100–104.

[14] J. Huang, L. Yang, D. Liu, J. Chen, Q. Fu, Y. Xiong, F. Lin, B. Xiang, Large-area synthesis of monolayer WSe₂ on a SiO₂/Si substrate and its device applications, *Nanoscale.* 7 (2015) 4193–4198. <https://doi.org/10.1039/c4nr07045c>.

[15] T. Wang, K. Andrews, A. Bowman, T. Hong, M. Koehler, J. Yan, D. Mandrus, Z. Zhou, Y.Q. Xu, High-Performance WSe₂ Phototransistors with 2D/2D Ohmic Contacts, *Nano Lett.* 18 (2018) 2766–2771. <https://doi.org/10.1021/acs.nanolett.7b04205>.

[16] Z. Wang, H.H. Wu, Q. Li, F. Besenbacher, Y. Li, X.C. Zeng, M. Dong, Reversing Interfacial Catalysis of Ambipolar WSe₂ Single Crystal, *Adv. Sci.* 7 (2020). <https://doi.org/10.1002/advs.201901382>.

[17] X. Huang, T. Wang, S. Miao, C. Wang, Z. Li, Z. Lian, T. Taniguchi, K. Watanabe, S. Okamoto, D.

Xiao, S.F. Shi, Y.T. Cui, Correlated insulating states at fractional fillings of the WS₂/WSe₂ moiré lattice, *Nat. Phys.* 17 (2021) 715–719. <https://doi.org/10.1038/s41567-021-01171-w>.

[18] S. Miao, T. Wang, X. Huang, D. Chen, Z. Lian, C. Wang, M. Blei, T. Taniguchi, K. Watanabe, S. Tongay, Z. Wang, D. Xiao, Y.T. Cui, S.F. Shi, Strong interaction between interlayer excitons and correlated electrons in WSe₂/WS₂ moiré superlattice, *Nat. Commun.* 12 (2021) 8–13. <https://doi.org/10.1038/s41467-021-23732-6>.

[19] P. Zhou, P. Schiettecatte, M. Vandichel, A. Rousaki, P. Vandenabeele, Z. Hens, S. Singh, Synthesis of Colloidal WSe₂ Nanocrystals: Polymorphism Control by Precursor-Ligand Chemistry, *Cryst. Growth Des.* 21 (2021) 1451–1460. <https://doi.org/10.1021/acs.cgd.0c01036>.

[20] T.H. Tsai, Z.Y. Liang, Y.C. Lin, C.C. Wang, K.I. Lin, K. Suenaga, P.W. Chiu, Photogating WS₂ Photodetectors Using Embedded WSe₂ Charge Puddles, *ACS Nano.* 14 (2020) 4559–4566. <https://doi.org/10.1021/acsnano.0c00098>.

[21] C. Huang, S. Wu, A.M. Sanchez, J.J.P. Peters, R. Beanland, J.S. Ross, P. Rivera, W. Yao, D.H. Cobden, X. Xu, Lateral heterojunctions within monolayer MoSe₂-WSe₂ semiconductors, *Nat. Mater.* 13 (2014) 1096–1101. <https://doi.org/10.1038/nmat4064>.

[22] S. Yu, Q. Rice, B. Tabibi, Q. Li, F.J. Seo, Piezoelectricity in WSe₂/MoS₂ heterostructure atomic layers, *Nanoscale.* 10 (2018) 12472–12479. <https://doi.org/10.1039/c8nr04394a>.

[23] J. Pouzet, J.C. Bernede, A. Khellil, H. Essaidi, S. Benhida, Preparation and characterization of tungsten diselenide thin films, *Thin Solid Films.* 208 (1992) 252–259. [https://doi.org/10.1016/0040-6090\(92\)90652-R](https://doi.org/10.1016/0040-6090(92)90652-R).

[24] S. Zhang, C.G. Wang, M.Y. Li, D. Huang, L.J. Li, W. Ji, S. Wu, Defect Structure of Localized Excitons in a WSe₂ Monolayer, *Phys. Rev. Lett.* 119 (2017) 1–6. <https://doi.org/10.1103/PhysRevLett.119.046101>.

- [25] D. Yang, X. Fan, F. Zhang, Y. Hu, Z. Luo, Electronic and Magnetic Properties of Defected Monolayer WSe₂ with Vacancies, *Nanoscale Res. Lett.* 14 (2019). <https://doi.org/10.1186/s11671-019-3002-2>.
- [26] H. Zeng, G. Bin Liu, J. Dai, Y. Yan, B. Zhu, R. He, L. Xie, S. Xu, X. Chen, W. Yao, X. Cui, Optical signature of symmetry variations and spin-valley coupling in atomically thin tungsten dichalcogenides, *Sci. Rep.* 3 (2013) 4908–4916. <https://doi.org/10.1038/srep01608>.
- [27] Z. Zheng, T. Zhang, J. Yao, Y. Zhang, J. Xu, G. Yang, Flexible, transparent and ultra-broadband photodetector based on large-area WSe₂ film for wearable devices, *Nanotechnology.* 27 (2016) 1–11. <https://doi.org/10.1088/0957-4484/27/22/225501>.
- [28] J.H. Park, S. Fathipour, I. Kwak, K. Sardashti, C.F. Ahles, S.F. Wolf, M. Edmonds, S. Vishwanath, H.G. Xing, S.K. Fullerton-Shirey, A. Seabaugh, A.C. Kummel, Atomic Layer Deposition of Al₂O₃ on WSe₂ Functionalized by Titanyl Phthalocyanine, *ACS Nano.* 10 (2016) 6888–6896. <https://doi.org/10.1021/acsnano.6b02648>.
- [29] L. Hu, X. Liu, S. Dagleish, M.M. Matsushita, H. Yoshikawa, K. Awaga, Organic optoelectronic interfaces with anomalous transient photocurrent, *J. Mater. Chem. C.* 3 (2015) 5122–5135. <https://doi.org/10.1039/C5TC00414D>.
- [30] L.M. Peter, Energetics and kinetics of light-driven oxygen evolution at semiconductor electrodes: The example of hematite, *J. Solid State Electrochem.* 17 (2013) 315–326. <https://doi.org/10.1007/s10008-012-1957-3>.
- [31] J. Wu, Z. Fan, J. Chen, X. Jiang, Atomic defects in monolayer WSe₂ tunneling FETs studied by systematic ab initio calculations, *Appl. Phys. Express.* 11 (2018) 54001. <https://doi.org/10.7567/APEX.11.054001>.

Highlights:

- Chemical vapor transport synthesis of WSe₂ from pre-deposited WO₃ and W precursor films
- Surface morphology and structure of as-prepared WSe₂ films were studied and compared
- Two-terminal photoconductor devices were fabricated and characterized

CRedit authorship contribution statement

Kevon Kadiwala: Methodology, Validation, Investigation, Visualization, Writing - original draft. **Edgars Butanovs:** Methodology, Investigation, Writing – review & editing. **Martins Zubkins:** Investigation. **Andrejs Ogurcovs:** Investigation. **Boris Polyakov:** Conceptualization, Supervision, Investigation, Writing - review & editing.

Journal Pre-proofs